

# Size-Sieving Separation of Hard-Sphere Mixtures through Cylindrical Pores

Yue Yu<sup>1</sup> and Kai Zhang<sup>1,2,\*</sup>

<sup>1</sup>*Division of Natural and Applied Sciences, Duke Kunshan University, Kunshan, Jiangsu, 215300, China*

<sup>2</sup>*Data Science Research Center (DSRC), Duke Kunshan University, Kunshan, Jiangsu, 215300, China*

(Dated: April 23, 2021)

The collision dynamics of hard spheres and cylindrical pores is solved exactly, which is the minimal model for a regularly porous membrane. Nonequilibrium event-driven molecular dynamics simulations are used to show that the permeability  $P$  of hard spheres of size  $\sigma$  through cylindrical pores of size  $d$  follow the hindered diffusion mechanism due to size exclusion as  $P \propto (1 - \sigma/d)^2$ . Under this law, the separation of binary mixtures of large and small particles exhibits a linear relationship between  $\alpha^{-1/2}$  and  $P^{-1/2}$ , where  $\alpha$  and  $P$  are the selectivity and permeability of the smaller particle, respectively. The mean permeability through polydisperse pores is the sum of permeabilities of individual pores, weighted by the fraction of the single pore area over the total pore area.

PACS numbers: 47.61.-k, 47.45.-n, 47.55.Mh, 47.56.+r, 83.10.Rs, 02.70.Ns

Membrane separation is an energy-efficient way to extract some substances from others with a multitude of industrial applications such as water desalination, ion exchange, carbon capture and protein purification [1]. The goal here is to maximize the acquisition rate of the desired species at the highest possible purity by effectively filtering out undesired ones. However, an intrinsic trade-off always exists between this pair of separation performance characteristics – permeability and selectivity [2]. Although different penetrants, being angstrom-sized (Å) ions/molecules, nanometer-sized (nm) macromolecules, or micrometer-sized ( $\mu\text{m}$ ) bacteria, may have different transport mechanisms, it is now generally believed that narrowing down the size distribution of membrane pores can achieve higher separation performance [3, 4]. Apart from widely-used microfiltration and ultrafiltration membranes [5], tremendous efforts have been made to prepare regularly porous structures on nano- or molecular scales in systems such as zeolites [6], metal organic frameworks [7] (MOFs), and silicon nanochannels [8]. Recent advances in self-assembly techniques further enabled the synthesis of ceramic [9], graphene-based [10] or block copolymer [11] molecular sieves, which are featured with well-controlled pores as regular as parallel cylinders. It is therefore needed to develop a quantitative understanding of how the steric (size) exclusion effect imposed by regular pores determines the separation of particles of different sizes.

In the early study of gas transport through long cylindrical tubes [12], it was found that the bulk self diffusivity  $D_s = \frac{1}{3}\lambda\bar{v}$  of a gas with molecular mass  $m$ , mean free path  $\lambda$  and mean velocity  $\bar{v} = \sqrt{\frac{8k_B T}{\pi m}}$  at temperature  $T$  becomes  $D_K = \frac{1}{3}d\bar{v}$  inside the tube, when the tube diameter  $d \ll \lambda$ . An implicit assumption of this Knudsen diffusion mechanism is that the diameter of gas molecules  $\sigma$  is much smaller than  $d$  so that they can be treated as point masses. If two gases were to be separated under Knudsen diffusion, it is the mass dependence

of  $D_K \sim \frac{1}{\sqrt{m}}$  that makes the heavier one exit the tube later, regardless of their sizes. More theoretical analysis showed that the transport diffusivity  $D$  of rarefied gases flowing under a density gradient also depends on the length of the tube  $L$  through the ratio  $L/d$  and  $D$  approaches  $D_K$  only when  $L \gg d$  [13–15]. But their conclusions are again limited to the case of  $\sigma \rightarrow 0$ . In the context of molecular sieves, we are more interested in the regime of  $\sigma \lesssim d$  where size exclusion takes effect. Although modifications to the Knudsen diffusion theory have been proposed to replace  $d$  with an effective diameter  $d_{\text{eff}} = d - \sigma$  expecting that  $D_K \propto d - \sigma$  [16], it is not clear whether this rule actually holds and whether the transport still remains Knudsen-like.

In this Letter, we study the transport and separation of low-density binary hard-sphere mixtures through cylindrical pores under a chemical potential gradient (Fig. 1). Each mixture consists of hard spheres  $A$  (large) and  $B$  (small) flowing from the upstream chamber 1 at chemical potential  $\mu_1$  to the downstream chamber 2 at a lower chemical potential  $\mu_2$ , implemented by the dual con-

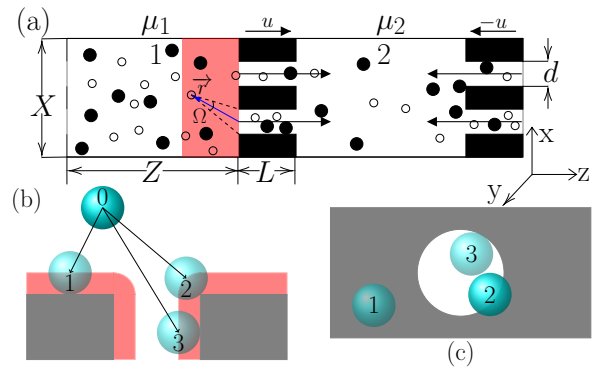


FIG. 1. (a) Simulation box setup of DCV-GCMD. A particle at position  $\mathbf{r}$  in the waiting zone (shaded) makes a solid angle  $\Omega$  to the pore opening. (b) Side and (c) top view of the three possible cases of particle-pore collision events.

control volume grand canonical molecular dynamics (DCV-GCMD) method [17, 18]. Previous molecular simulations on similar problems have mostly focused on Lennard-Jones like particles under slit-shaped confinement [19–25], and in consequence, were not able to distinguish size sieving from other effects. Other methods resort to equilibrium and/or stochastic sampling [26, 27] that cannot genuinely reflect the nonequilibrium transport dynamics driven by pressure gradients. To understand size-sieving filtration through regularly porous membranes, it is imperative to faithfully simulate the entrance of particles into pores. We analytically resolve the collision dynamics of hard spheres and cylindrical pores by considering three possibilities (Fig. 1(b-c)). A hard sphere can hit the membrane surface and bounce back (case 1), or hit the circular edge of the pore and then bounce away (case 2), or directly fly into the pore and hit its interior wall (case 3). We can compute the particle-pore collision time by considering the excluded volume of a sphere over the pore surface (red shaded area in Fig. 1(b)). The final solution is about finding the intersection between a linear path and a torus as in the problem of ray tracing in computer graphics [28, 29].

We set the diameter  $\sigma_A$  of  $A$  particles as the unit of length. The simulation box has dimensions of  $Z = 60$  and  $X = Y = 42$  with membrane thickness  $L = 20$  (Fig. 1(a)). Periodic boundary conditions are imposed along all directions such that particles can fly from chamber 1 to 2 through the two membranes in the box with opposite streaming velocities  $u$  and  $-u$ . We first pack monodisperse cylindrical pores in parallel on a square lattice with diameters ranging from  $d = 1.05$  to  $3.5$ . The number of pores on the membrane are adjusted to keep the total pore area  $S$  (or porosity) constant. The diameter of the smaller particle  $B$  spans over a wide range from  $\sigma_B = 0.95$  down to  $0.005$ . We use  $\mu_1 = -5$  and  $\mu_2 = -5.5, -\infty$  (particle sink), which maintain a number density  $\rho_1 \lesssim 0.007$  and  $\rho_2 \lesssim 0.004$  for each of the two components. The systems under study are thus gaseous for which ideal gas law about pressure holds, i.e.  $p = \rho k_B T$ . Estimation to the mean free path  $\lambda = \frac{k_B T}{\sqrt{2}\pi\sigma^2 p}$  and Knudsen number  $K_n = \lambda/d$  reveals that our systems are within or close to the free molecular flow regime.

The particle flux  $J$  (the number of particles going through a membrane per unit pore area per unit time) is calculated from the difference between the net insertion/removal numbers in the two chambers [17] or from the number of particle crossing events in each pore. Instead of using the transport diffusivity  $D$  defined by the Fick's law  $J = -D \frac{\Delta p}{L}$ , we report the transport *permeability*  $P$  defined by  $J = -P \frac{\Delta p}{L} = -P \nabla p$  and at the low densities of this work  $D \approx P k_B T$ . We find that, for all the particle sizes  $\sigma$  and pore sizes  $d$  under study,  $P(d, \sigma)$  collapse onto a universal curve when plotted as a function of the ratio  $\sigma/d$  (Fig. 2). It can be numerically verified

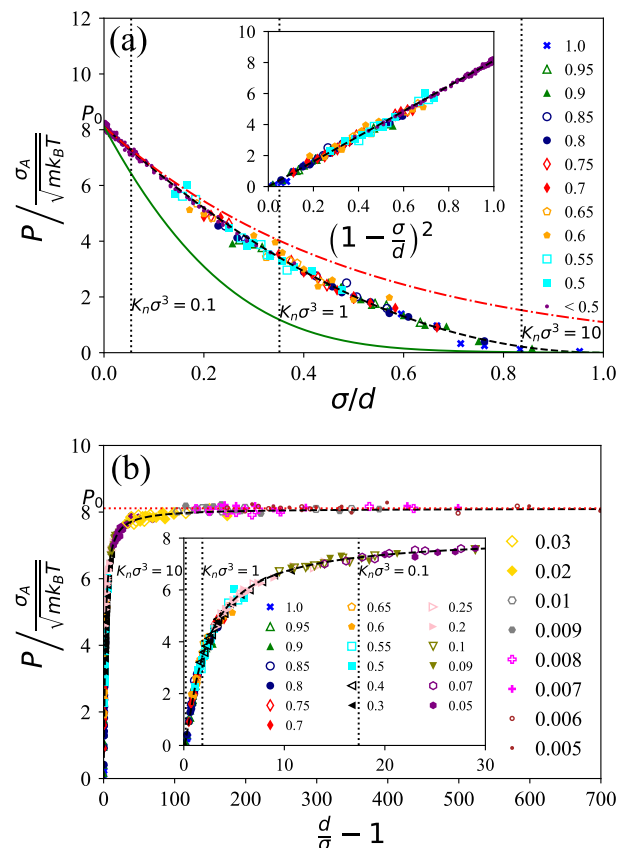


FIG. 2. Permeability of hard spheres of size  $\sigma$  (indicated by different symbols) through pores of diameter  $d = 1.05 - 3.5$ , following the hindered diffusion law  $P = P_0(1 - \frac{\sigma}{d})^2$  (black dashed). (a) Exponential law  $P = P_0 \exp(-2\sigma/d)$  is approximately obeyed for small  $\sigma/d$  (red dotted-dashed). Renkin's law does not apply here (green solid). (b)  $P$  shows apparent linearity for small  $\frac{d}{\sigma} - 1$  but saturates at  $P_0$  as  $\sigma/d \rightarrow 0$ . Vertical dotted lines mark the boundaries at  $K_n \sigma^3 = 0.1, 1.0, 10$ .

that the hindered diffusion law [30]

$$P(d, \sigma) = P_0 \left(1 - \frac{\sigma}{d}\right)^2 \quad (1)$$

is obeyed with a fitting coefficient  $P_0 \approx 8$ . The geometric factor  $(1 - \frac{\sigma}{d})^2$  simply originates from the accessible area  $\pi(d - \sigma)^2/4$  for a particle to enter the circular opening. Usually, hindered diffusion describes the transport of large particles in liquid solvent [31], and due to hydrodynamic effect, an extra factor needs to be included as in the Renkin's law  $P = P_0(1 - \frac{\sigma}{d})^2 \left(1 - 2.104 \frac{\sigma}{d} + 2.09 \frac{\sigma^3}{d^3} - 0.95 \frac{\sigma^5}{d^5}\right)$  [32]. For solvent-free gaseous particles, the geometric factor alone can determine the permeability (Fig. 2(a)). When viewed as a function of  $d - \sigma$  or  $\frac{d}{\sigma} - 1$ ,  $P$  shows apparent linearity when  $\sigma$  is comparable with  $d$ . But such linearity is just the numerical consequence of the hindered diffusion law, i.e.  $(1 - \sigma/d)^2 = \left[1 - \frac{1}{1+(d/\sigma-1)}\right]^2 = \frac{(d/\sigma-1)^2}{[1+(d/\sigma-1)]^2}$ .

Around  $\frac{d}{\sigma} - 1 \rightarrow 0$ , the trend of  $P$  is actually curved as  $\sim (d/\sigma - 1)^2$ . In the limit of  $\sigma \ll d$ , instead of having a Knudsen-like diffusion with  $P \sim d$ , we observe that  $P$  saturates at a constant  $P_0$  (Fig. 2(b)).

The front factor  $P_0$  in our result can be understood by considering the net flux of point particles through the circular opening at each pore. On average, half of the particles move from chamber 1 to 2 with a streaming velocity  $u$  and it takes  $\tau = L/u$  for all the  $N$  particles inside a pore to be emitted to chamber 2. Meanwhile, there must be another  $N$  particles entering that pore from chamber 1 at steady state, which are originally in the “waiting” zone of thickness  $L$  next to the pore opening (red shaded area in Fig. 1(a)). We can choose the waiting zone to be a cylinder of volume  $V$  with a height  $L$  and a radius  $\infty$ . The probability that a particle at a given point  $\mathbf{r}$  in this region to enter the pore is determined by the solid angle  $\Omega(\mathbf{r})$  made from  $\mathbf{r}$  to the circular pore opening of an area  $s = \pi d^2/4$ . If we assume  $\rho_1 = \rho$  and  $\rho_2 = 0$  for simplicity, then  $N = \rho \int_V d\mathbf{r} \frac{\Omega(\mathbf{r})}{4\pi} = \frac{\rho}{4\pi} I(d, L)$ , where the

integral  $I(d, L) = \int_0^\infty r dr \int_0^{2\pi} d\theta \int_0^L dz \Omega(r, \theta, z)$  can be evaluated numerically for given  $d$  and  $L$  [33]. The permeability or diffusivity for point particles can thus be estimated as  $P_0 k_B T = D_0 = \frac{N}{s\tau} \frac{\Delta p}{L} = \frac{I u}{\pi^2 d^2}$ . For  $L = 20$ , we find  $\frac{I}{\pi^2 d^2} = 10.0$  and if we make the approximation that  $u \approx \langle |v_z| \rangle = \sqrt{\frac{2k_B T}{\pi m}} \approx 0.798$ ,  $P_0 \approx 7.98$  which is close to the result of numerical fitting in Eq. (1).

Having confirmed the hindered diffusion mechanism, we can predict the separation curves for binary gaseous mixtures through cylindrical pores as

$$\alpha = \frac{1}{\left[ \frac{\sigma_A}{\sigma_B} - \sqrt{P_0} \left( \frac{\sigma_A}{\sigma_B} - 1 \right) P_B^{-1/2} \right]^2} \quad (2)$$

where  $\alpha \equiv \frac{P_B}{P_A} > 1$  is the (ideal) *selectivity* of the more permeable gas  $B$  (smaller) with respect to the less permeable one  $A$  (Fig. 3). In industry, majority of the gas separation membranes are rubbery or glassy polymers, in which gases transport with an activated diffusion mechanism  $D \sim \exp(-\frac{a\sigma^2}{k_B T})$  [34, 35]. As a result, the “upper bound” of selectivity versus permeability empirically satisfies the linear relationship  $\log \alpha = -\lambda_{AB} \log P_B + \kappa$ , whose slope was shown to be  $\lambda_{AB} = \lambda_F \equiv \left( \frac{\sigma_A}{\sigma_B} \right)^2 - 1$  [36, 37]. Although there is no strict linear relationship on log-log scale from Eq. (2), it can be shown that, for small  $\sigma/d$ ,  $\log \alpha \approx -\lambda_{AB} \log P_B + \lambda_{AB} \log P_0$  with  $\lambda_{AB} = \frac{\sigma_A}{\sigma_B} - 1$  because  $P \approx P_0 \exp(-2\sigma/d)$ . The true linear relationship over the entire regime of  $\sigma/d$  is between  $\alpha^{-1/2}$  and  $P_B^{-1/2}$ , i.e.

$$\alpha^{-1/2} = \frac{\sigma_A}{\sigma_B} - \sqrt{P_0} \left( \frac{\sigma_A}{\sigma_B} - 1 \right) P_B^{-1/2}. \quad (3)$$

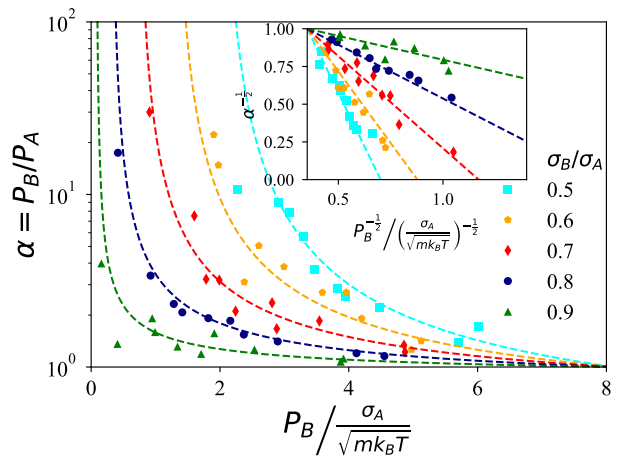


FIG. 3. Selectivity  $\alpha$  versus permeability  $P_B$  for binary hard spheres of various size ratios  $\sigma_B/\sigma_A$ . Inset shows the linear relationship between  $\alpha^{-1/2}$  and  $P_B^{-1/2}$ .

Pore sizes in real membranes are inevitably polydisperse. We consider variation of  $d$  subject to the log-normal distribution  $f(d; \bar{d}, \delta)$  with mean  $\bar{d}$  and standard deviation  $\delta \bar{d}$  ( $\delta$  is called *polydispersity*)

$$f(d; \bar{d}, \delta) = \frac{1}{d \sqrt{2\pi \ln(1 + \delta^2)}} e^{-\frac{[\ln(d\sqrt{1+\delta^2}/\bar{d})]^2}{2 \ln(1+\delta^2)}}.$$

At a pressure gradient  $\nabla p$ , the total number  $N$  of particles going through all pores during time  $\tau$  should equal to the sum of number  $N_i$  of particles going through each pore  $i$  with an area  $s_i$ , i.e.  $N = \bar{P} \nabla p S \tau = \sum_i P_i \nabla p s_i \tau = \sum_i N_i$ . If we assume the permeability for each pore of size  $d_i$  is  $P_i = P_0 (1 - \sigma/d_i)^2$ , then  $N_i \propto P_i s_i = (1 - \sigma/d_i)^2 d_i^2 = (d_i - \sigma)^2$ . Simulations using polydisperse membranes with  $\delta = 0.2$  and  $\bar{d} = 1.05$ – $3.5$  show that  $N_i$  is indeed proportional to  $(d_i - \sigma)^2$  (Fig. 4(a)).

The mean permeability  $\bar{P} = \sum_i P_i \frac{s_i}{S} = \sum_i P_i \frac{d_i^2}{\sum_i d_i^2}$ , for a continuous distribution  $f(d; \bar{d}, \delta)$  of  $d$ , can thus be calculated as

$$\bar{P}_\delta(\bar{d}, \sigma) = \frac{\int_\sigma^\infty f(d; \bar{d}, \delta) P(d, \sigma) d^2 dd}{\int_\sigma^\infty f(d; \bar{d}, \delta) d^2 dd}, \quad (4)$$

after knowing the monodisperse permeability  $P(d, \sigma)$  as a function of  $d$  and  $\sigma$  (Fig. 4(b)). Here, the weight in the average calculation is  $d^2$ , which differs from  $d^4$  in viscous (Hagen-Poiseuille) flows [5]. Eq. (4) can be used to predict permeability enhancement  $\bar{P}_{0,0}/\bar{P}_\delta$  at a given selectivity or selectivity enhancement  $\alpha_{0,0}/\alpha_\delta$  at a given mean pore size  $\bar{d}$ , when we narrow down the pore size distribution from  $\delta > 0$  to 0.0 (monodisperse) as shown in Fig. 4(c)-(d).

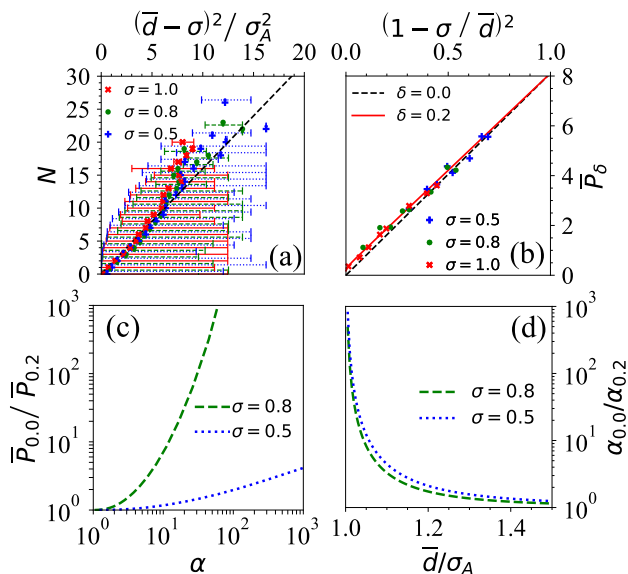


FIG. 4. (a) Number  $N$  of particles (of size  $\sigma_A = 1.0$  and  $\sigma_B = 0.8, 0.5$ ) going through pores of different diameter  $d$  during simulations using polydisperse membranes. Horizontal line-bars enclose the range of  $d$ 's for a given  $N$  and  $\bar{d}$  is their average.  $N$  is proportional to  $(\bar{d} - \sigma)^2$  (black dashed line which is a guide to the eye). (b) The average permeability  $\bar{P}_\delta$  of the three types of particles going through cylindrical pores with polydispersity  $\delta$ . Solid line is calculated using the ansatz that the contribution from a pore of size  $d$  should be weighted by  $d^2$ . (c) Calculated permeability enhancement as a function of selectivity and (d) calculated selectivity enhancement as a function of the mean pore size  $\bar{d}$  of the polydisperse membrane, to separate binary mixtures of  $\sigma_A = 1$  and  $\sigma_B = 0.8, 0.5$ .

The interests in transport and separation are not limited to free molecular flows ( $K_n > 10^1$ ), but have also been directed to continuum ( $K_n < 10^{-3}$ ), slip ( $10^{-3} < K_n < 10^{-1}$ ) and transition flows ( $10^{-1} < K_n < 10^1$ ) [38]. Decades ago, it was thought that molecular simulations are computationally too expensive to address these regimes when the number of particles is large. Approximate theoretical models or computational methods were thus developed to tackle these problems, such as the dusty-gas model (DGM) [39], the direct simulation Monte Carlo (DSMC) [40, 41] and the finite element method [42]. With the ever-increasing computer power, it now becomes more and more promising to investigate dense flows on particle level [43, 44]. It would be interesting to extend the current methodology to low-Kn porous systems. Caution should be taken when applying the model used in this work to molecular systems, because the intrinsic roughness of atomic packings, which can induce back reflection and dissipation, are not captured by smooth cylindrical walls [27, 45].

We thank M. Ronen Plesser for helpful discussions on solid angle calculation. We acknowledge support from

Duke Kunshan startup funding. This work also benefited from resources made available at the Duke Compute Cluster (DCC) and the Kunshan Supercomputing Center (KSSC).

\* kai.zhang@dukekunshan.edu.cn

- [1] R. W. Baker, *Membrane Technology and Applications* (John Wiley & Sons, 2012).
- [2] H. B. Park, J. Kamcev, L. M. Robeson, M. Elimelech, and B. D. Freeman, *Science* **356** (2017).
- [3] J. D. Moon, B. D. Freeman, C. J. Hawker, and R. A. Segalman, *Macromolecules* **53**, 5649 (2020).
- [4] T. E. Culp, B. Khara, K. P. Brickey, M. Geitner, T. J. Zimudzi, J. D. Wilbur, S. D. Jons, A. Roy, M. Paul, B. Ganapathysubramanian, *et al.*, *Science* **371**, 72 (2021).
- [5] A. Mehta and A. L. Zydney, *J. Membr. Sci.* **249**, 245 (2005).
- [6] B. Smit and T. L. Maesen, *Chem. Rev.* **108**, 4125 (2008).
- [7] S. Qiu, M. Xue, and G. Zhu, *Chem. Soc. Rev.* **43**, 6116 (2014).
- [8] S. Gruener and P. Huber, *Phys. Rev. Lett.* **100**, 064502 (2008).
- [9] C. Kresge, M. Leonowicz, W. J. Roth, J. Vartuli, and J. Beck, *Nature* **359**, 710 (1992).
- [10] H. Li, Z. Song, X. Zhang, Y. Huang, S. Li, Y. Mao, H. J. Ploehn, Y. Bao, and M. Yu, *Science* **342**, 95 (2013).
- [11] W. A. Phillip, J. Rzyayev, M. A. Hillmyer, and E. Cussler, *J. Membr. Sci.* **286**, 144 (2006).
- [12] M. Knudsen, *Annalen der Physik* **333**, 75 (1909).
- [13] W. Pollard and R. D. Present, *Phys. Rev.* **73**, 762 (1948).
- [14] Y. Shi, Y. T. Lee, and A. S. Kim, *Transport in Porous Media* **93**, 517 (2012).
- [15] F. Colson and D. A. Barlow, *Phys. Rev. E* **100**, 062125 (2019).
- [16] J. Gilron and A. Soffer, *J. Membr. Sci.* **209**, 339 (2002).
- [17] G. S. Heffelfinger and D. M. Ford, *Mol. Phys.* **94**, 659 (1998).
- [18] D. M. FORD and G. S. HEFFELFINGER, *Mol. Phys.* **94**, 673 (1998).
- [19] R. F. Cracknell, D. Nicholson, and N. Quirke, *Phys. Rev. Lett.* **74**, 2463 (1995).
- [20] S.-i. Furukawa, T. Shigeta, and T. Nitta, *J. Chem. Eng. Japan* **29**, 725 (1996).
- [21] S.-i. Furukawa and T. Nitta, *J. Chem. Eng. Japan* **30**, 116 (1997).
- [22] S.-i. Furukawa, K. Hayashi, and T. Nitta, *J. Chem. Eng. Japan* **30**, 1107 (1997).
- [23] L. Xu, M. G. Sedigh, M. Sahimi, and T. T. Tsotsis, *Phys. Rev. Lett.* **80**, 3511 (1998).
- [24] L. Xu, M. Sahimi, and T. T. Tsotsis, *Phys. Rev. E* **62**, 6942 (2000).
- [25] H. Takaba, K. Mizukami, M. Kubo, A. Fahmi, and A. Miyamoto, *AIChE Journal* **44**, 1335 (1998).
- [26] K. Mon and J. K. Percus, *J. Chem. Phys.* **117**, 2289 (2002).
- [27] K. Malek and M.-O. Coppens, *J. Chem. Phys.* **119**, 2801 (2003).
- [28] E. Lengyel, *Mathematics for 3D game programming and computer graphics* (Cengage Learning PTR, Boston,

- 2012).
- [29] See Supplemental Material for simulation details.
- [30] R. E. Beck and J. S. Schultz, *Science* **170**, 1302 (1970).
- [31] W. Deen, *AIChE Journal* **33**, 1409 (1987).
- [32] E. M. Renkin, *J. Gen. Physiol.* **38**, 225 (1954).
- [33] F. Paxton, *Rev. Sci. Instrum.* **30**, 254 (1959).
- [34] K. Ghosal and B. D. Freeman, *Polym. Adv. Technol.* **5**, 673 (1994).
- [35] A. A. Gusev, S. Arizzi, U. W. Suter, and D. J. Moll, *J. Chem. Phys.* **99**, 2221 (1993).
- [36] L. M. Robeson, *J. Membr. Sci.* **62**, 165 (1991).
- [37] B. D. Freeman, *Macromolecules* **32**, 375 (1999).
- [38] J. Welty, G. L. Rorrer, and D. G. Foster, *Fundamentals of momentum, heat, and mass transfer* (John Wiley & Sons, 2015).
- [39] E. Mason, A. Malinauskas, and R. Evans Iii, *J. Chem. Phys.* **46**, 3199 (1967).
- [40] G. Bird, *Phys. Fluids* **6**, 1518 (1963).
- [41] F. J. Alexander and A. L. Garcia, *Comput. Phys.* **11**, 588 (1997).
- [42] S. Roy, R. Raju, H. F. Chuang, B. A. Cruden, and M. Meyyappan, *J. Appl. Phys.* **93**, 4870 (2003).
- [43] S. Plimpton, *J. Comput. Phys.* **117**, 1 (1995).
- [44] Q. Sheng, L. Gibelli, J. Li, M. K. Borg, and Y. Zhang, *Phys. Fluids* **32**, 092003 (2020).
- [45] G. Arya, H.-C. Chang, and E. J. Maginn, *Phys. Rev. Lett.* **91**, 026102 (2003).